Preprints of the 19th World Congress
The International Federation of Automatic Control
Cape Town, South Africa. August 24-29, 2014

Nonlinear Physics-model-based Actuator Trajectory Optimization for Advanced Scenario Planning in the DIII-D Tokamak ⋆

Justin E. Barton * **Wenyu Shi** * **Eugenio Schuster** *
Tim C. Luce ** **John R. Ferron** ** **Michael L. Walker** **
David A. Humphreys ** **Francesca Turco** ***
Robert D. Johnson ** **Ben G. Penaflor** **

* *Lehigh University, Bethlehem, PA 18015, USA.*
** *General Atomics, San Diego, CA 92121, USA.*
*** *Columbia University, New York, NY 10027, USA.*

Abstract: Extensive research has been conducted to find operating scenarios that optimize the plasma performance in nuclear fusion tokamak devices with the goal of enabling the success of the ITER project. The development, or planning, of these advanced scenarios is traditionally investigated experimentally by modifying the tokamak's actuator trajectories, such as the auxiliary heating/current-drive (H&CD) scheme, and analyzing the resulting plasma evolution. In this work, a numerical optimization algorithm is developed to complement the experimental effort of advanced scenario planning in the DIII-D tokamak. Two properties related to the plasma stability and performance are the safety factor profile (q-profile) and the normalized plasma beta (β_N). The optimization algorithm goal is to design actuator trajectories that steer the plasma to a target q-profile and plasma β_N, such that the achieved state is stationary in time, subject to the plasma dynamics (described by a physics-based, nonlinear, control-oriented partial differential equation model) and practical plasma state and actuator constraints, such as the maximum available amount of H&CD power. This defines a nonlinear, constrained optimization problem that we solve by employing sequential quadratic programming. The optimized trajectories are then tested through simulation with the physics-based model and experimentally in DIII-D.

1. INTRODUCTION

The goal of a commercial grade nuclear fusion reactor is to create the conditions necessary for the reactant nuclei (typically deuterium and tritium in a future reactor-grade device) to have a significant probability of "fusing" together and releasing energy in the process. In order for the reactant nuclei to fuse, they must possess enough kinetic energy to overcome the Coulombic repulsion force that exists between them. This is accomplished by heating the nuclei to extremely high temperatures, which results in the reactants being in the plasma state. The magnetic confinement approach to nuclear fusion is predicated on exploiting the plasma's ability to conduct electrical current and interact with magnetic fields. In the tokamak magnetic confinement device (Wesson (2004)), externally applied magnetic fields are utilized to confine the plasma in a fixed volume and create the conditions necessary for fusion to occur. The next step in the development of the tokamak concept to fusion energy production is the ITER project.

A significant research thrust has been ongoing in the tokamak fusion community to find advanced, high performance operating scenarios with the goal of developing candidate scenarios for ITER (Taylor et al. (1997)). These scenarios are characterized by a high fusion gain, good plasma confinement, magnetohydrodynamic (MHD) stability, and a noninductively driven plasma current. The development of these advanced scenarios is experimentally explored by specifying the device's actuator trajectory waveforms, such as the total plasma current and auxiliary heating and current-drive (H&CD) sources, and analyzing the resulting plasma evolution (conventionally referred to as advanced scenario planning). Traditionally, these feedforward actuator trajectories are developed through a substantial number of trial-and-error attempts and based on extensive experience gained during operation of a particular device. Two properties often used to define a plasma scenario are the safety factor profile (q-profile), which is related to the plasma stability and performance, and the normalized plasma beta (β_N), which is a measure of the confinement efficiency of a plasma equilibrium (Wesson (2004)).

In this work, we develop a numerical optimization algorithm to complement the experimental effort of advanced scenario planning in the DIII-D tokamak. In Barton et al. (2013), a physics-based, control-oriented partial differential equation (PDE) model of the evolution of the poloidal magnetic flux profile (related to the q-profile) valid for advanced, high confinement (H-mode) scenarios (Wesson (2004)) was developed. High confinement tokamak scenarios are characterized by transport barriers (Wesson (2004)) just inside the plasma boundary that increase the coupling between the plasma magnetic and kinetic states through the increase of the bootstrap current (a

⋆ This work was supported by the U.S. Department of Energy (DE-SC0001334, DE-SC0010661 and DE-FC02-04ER54698). E-mail contact of first author: justin.barton@lehigh.edu

self-generated current) (Peeters (2000)). The evolution of the plasma stored energy (related to the plasma β_N) is modeled by a volume-averaged energy balance equation. These nonlinear, physics-based models are embedded in a constrained optimization algorithm to determine actuator trajectories that steer the plasma to a particular target state at a predefined time during the plasma discharge. The proximity of the achieved plasma state to the predefined target is formulated into a cost functional to be minimized. The target state is chosen to be defined in terms of the achieved q-profile, plasma β_N, and the time stationarity of the achieved state, the latter of which is included to ensure the plasma remains at the desired operating point. Additionally, actuator constraints, such as the maximum amount of auxiliary H&CD power and the total plasma current ramp rate, and plasma state constraints, such as the minimum value of the q-profile (to avoid the onset of MHD instabilities that degrade the plasma performance), are imposed on the optimization problem solution. The nonlinear, constrained, optimization problem is then to design actuator trajectories that minimize the cost functional subject to the plasma dynamics and the actuator and plasma state constraints. We numerically solve this optimization problem by employing sequential quadratic programming (Nocedal and Wright (2006)). Previous advances in actuator trajectory optimization in low confinement (L-mode) scenarios (Wesson (2004)) in the DIII-D and TCV tokamaks can be found in Ou et al. (2008); Xu et al. (2010); Felici et al. (2012). Finally, the optimized trajectories are tested through simulation with the physics-based model and experimentally in DIII-D. In the studied scenarios, the plasma has transitioned from L-mode to H-mode prior to the utilization of the optimized trajectories, i.e., the trajectories are only designed for the high performance phase of the discharge.

2. PLASMA POLOIDAL MAGNETIC FLUX PROFILE AND STORED ENERGY EVOLUTION MODELS

In a well confined tokamak plasma, nested surfaces of constant poloidal magnetic flux are obtained and any quantity that is constant on each surface can be used to index them. In this work, the mean effective minor radius, ρ, of the magnetic flux surface, i.e., $\Phi = \pi B_{\phi,0}\rho^2$, is chosen as the indexing variable, where Φ is the toroidal magnetic flux and $B_{\phi,0}$ is the vacuum toroidal magnetic field at the geometric major radius R_0 of the tokamak. The normalized effective minor radius is defined as $\hat{\rho} = \rho/\rho_b$, where ρ_b is the mean effective minor radius of the last closed magnetic flux surface.

There are many plasma parameters that are of interest in determining the stability and performance of a tokamak operating scenario. We give as examples, the q-profile, the plasma β_N, and the plasma loop-voltage profile, U_p. The q-profile is related to the spatial gradient of the poloidal magnetic flux Ψ and is defined as

$$q(\hat{\rho},t) = -d\Phi/d\Psi = -(B_{\phi,0}\rho_b^2\hat{\rho})/(\partial\psi/\partial\hat{\rho}), \qquad (1)$$

where t is the time and ψ is the poloidal stream function, which is closely related to the poloidal flux ($\Psi = 2\pi\psi$). The plasma β_N is related to the volume-averaged plasma stored energy E and is defined as

$$\beta_N = \beta_t[\%]\frac{aB_{\phi,0}}{I_p} \quad \beta_t = \frac{\langle p\rangle_V}{B_{\phi,0}^2/(2\mu_0)} = \frac{(2/3)(E/V_p)}{B_{\phi,0}^2/(2\mu_0)}, \qquad (2)$$

where β_t is the toroidal plasma beta (Wesson (2004)), a is the plasma minor radius, I_p is the total plasma current (evaluated in units of MA), p is the plasma kinetic pressure, $\langle\cdot\rangle_V$ denotes the volume-average operation $1/V_p\int_V(\cdot)dV$, V is the volume enclosed by a magnetic flux surface, V_p is the total plasma volume, and μ_0 is the vacuum magnetic permeability. The loop-voltage profile is related to the temporal derivative of the poloidal magnetic flux and is defined as

$$U_p(\hat{\rho},t) = -\partial\Psi/\partial t = (-2\pi)\partial\psi/\partial t. \qquad (3)$$

From (1)-(3), we see that the q-profile, plasma β_N, and loop-voltage profile are related to the plasma magnetic and thermal states, ψ and E, respectively.

In Barton et al. (2013), a general simplified physics-based modeling approach has been developed to convert the first-principles physics model that describes the plasma poloidal magnetic flux profile evolution (the magnetic diffusion equation (Hinton and Hazeltine (1976))) into a form suitable for control design, with emphasis on H-mode scenarios. The nonlinear, physics-based PDE model of the poloidal flux evolution assumes the magnetic flux surface geometry is fixed and has subsequently been tailored to DIII-D and is expressed as (Barton et al. (2013))

$$\frac{\partial\psi}{\partial t} = f_\eta(\hat{\rho})\,u_\eta(t)\frac{1}{\hat{\rho}}\frac{\partial}{\partial\hat{\rho}}\left(\hat{\rho}D_\psi(\hat{\rho})\frac{\partial\psi}{\partial\hat{\rho}}\right) + \sum_{i=1}^{n_{ec}} f_{ec_i}(\hat{\rho})\,u_{ec_i}(t) + \sum_{i=1}^{n_{nbi}} f_{nbi_i}(\hat{\rho})\,u_{nbi_i}(t) + f_{bs}(\hat{\rho})\,u_{bs}(t)\left(\frac{\partial\psi}{\partial\hat{\rho}}\right)^{-1}, \qquad (4)$$

with boundary conditions

$$\partial\psi/\partial\hat{\rho}|_{\hat{\rho}=0} = 0 \qquad \partial\psi/\partial\hat{\rho}|_{\hat{\rho}=1} = -k_{I_p}u_{I_p}(t), \qquad (5)$$

where f_η, f_{ec_i}, f_{nbi_i}, and f_{bs} are functions of space, D_ψ pertains to the magnetic configuration of a particular plasma equilibrium, n_{ec} and n_{nbi} are the number of electron cyclotron (gyrotron) microwave launchers and neutral beam injectors, both of which are auxiliary H&CD actuators, respectively, and k_{I_p} is a constant. The diffusivity, interior, and boundary control terms are expressed as

$$\begin{aligned}
u_\eta(t) &= \left[I_p(t)P_{tot}(t)^{1/2}\bar{n}_e(t)^{-1}\right]^{-3/2},\\
u_{ec_i}(t) &= \left[I_p(t)P_{tot}(t)^{1/2}\bar{n}_e(t)^{-1}\right]^{-1/2}\bar{n}_e(t)^{-1}P_{ec_i}(t),\\
u_{nbi_i}(t) &= \left[I_p(t)P_{tot}(t)^{1/2}\bar{n}_e(t)^{-1}\right]^{-1}\bar{n}_e(t)^{-1}P_{nbi_i}(t),\\
u_{bs}(t) &= \left[I_p(t)P_{tot}(t)^{1/2}\bar{n}_e(t)^{-1}\right]^{-1/2}\bar{n}_e(t),\\
u_{I_p}(t) &= I_p(t),
\end{aligned} \qquad (6)$$

where $P_{tot}(t) = P_{ohm}(t) + \sum_{i=1}^{n_{ec}}P_{ec_i}(t) + \sum_{i=1}^{n_{nbi}}P_{nbi_i}(t) - P_{rad}(t)$ is the total power injected into the plasma, $P_{ohm}(t)$ is the ohmic power, $P_{ec_i}(t)$ and $P_{nbi_i}(t)$ are the individual gyrotron launcher and neutral beam injection powers, respectively, $P_{rad}(t)$ is the radiated power, and $\bar{n}_e(t)$ is the line-averaged electron density. Simplified physics-based models of the ohmic and radiated power are discussed in Barton et al. (2013). The volume-averaged plasma energy balance is given by

$$\frac{dE}{dt} = -\frac{E}{\tau_E(t)} + P_{tot}(t), \qquad (7)$$

where $\tau_E(t)$ is the global energy confinement time. The energy confinement time scaling used in this work is the IPB98(y,2) scaling law (ITER Physics Basis (1999)).

3. FORMULATION OF ACTUATOR TRAJECTORY OPTIMIZATION PROBLEM

3.1 Target Plasma State: Cost Functional Definition

The goal of the actuator trajectory optimization problem is to reach a target plasma state (defined in terms of the q-profile ($q^{tar}(\hat{\rho})$) and normalized plasma beta (β_N^{tar})) at some time t_f during the plasma discharge in such a way that the achieved state is as stationary in time as possible. As the poloidal flux profile evolves with the slowest time constant in the plasma, if it reaches a stationary condition, i.e., $U_p(\hat{\rho},t) = \text{constant}$, all of the other plasma profiles have also reached a stationary condition. If $U_p(\hat{\rho},t) = 0$, the total plasma current is completely driven by noninductive sources and this is referred to as a "steady-state" scenario. Therefore, the stationarity of the plasma state can be defined by the profile $g_{ss}(\hat{\rho},t) = \partial U_p/\partial\hat{\rho}$, and a stationary state is reached when $g_{ss}(\hat{\rho},t) = 0$. The proximity of the achieved plasma state to the target state at the time t_f can be described by the cost functional

$$J(t_f) = k_{ss}J_{ss}(t_f) + k_qJ_q(t_f) + k_{\beta_N}J_{\beta_N}(t_f), \quad (8)$$

where k_{ss}, k_q, and k_{β_N} are used to weight the relative importance of the plasma state characteristics and $J_q(t_f) = \int_0^1 W_q(\hat{\rho})\left[q^{tar}(\hat{\rho}) - q(\hat{\rho},t_f)\right]^2 d\hat{\rho}$, $J_{ss}(t_f) = \int_0^1 W_{ss}(\hat{\rho})\left[g_{ss}(\hat{\rho},t_f)\right]^2 d\hat{\rho}$, and $J_{\beta_N}(t_f) = \left[\beta_N^{tar} - \beta_N(t_f)\right]^2$, where $W_q(\hat{\rho})$ and $W_{ss}(\hat{\rho})$ are positive functions used to weight which portions of the respective profiles are more important relative to the others.

3.2 Plasma State Dynamics: Model Reduction via Spatial Discretization

To simulate the physics-based model, we spatially discretize the infinite dimensional PDE (4)-(5) by employing a finite difference method, where the spatial domain ($\hat{\rho} \in [0,1]$) is represented by m_ψ discrete nodes. After spatially discretizing (4) and taking into account the boundary conditions (5), we obtain a nonlinear finite dimensional ordinary differential equation (ODE) model defined by

$$\dot{\hat{\psi}} = f_\psi(\hat{\psi},u),$$

where $\hat{\psi} = [\psi_2,\ldots,\psi_{m_\psi-1}]^T \in \mathbb{R}^{n_\psi}$ is the magnetic state vector, ψ_i, for $i = 2,\ldots,m_\psi-1$, is the value of ψ at the i-th node, $u = [P_{ec_1},\ldots,P_{ec_{n_{ec}}},P_{nbi_1},\ldots,P_{nbi_{n_{nbi}}},\bar{n}_e,I_p]^T \in \mathbb{R}^{n_{act}}$ is the control input vector, $n_{act} = n_{ec} + n_{nbi} + 2$, $f_\psi \in \mathbb{R}^{n_\psi}$ is a nonlinear function of the plasma magnetic states and control inputs, and $n_\psi = m_\psi - 2$. By defining the plasma state vector as $x = [\hat{\psi},E] \in \mathbb{R}^{(n_\psi+1)}$, we can write the magnetic and kinetic state dynamics as

$$\dot{x} = \begin{bmatrix} f_\psi(\hat{\psi},u) \\ -\dfrac{E}{\tau_E(t)} + P_{tot}(x,u) \end{bmatrix} = F_{\psi,E}(x,u) \in \mathbb{R}^{(n_\psi+1)}. \quad (9)$$

We then integrate (9) in time by employing a fully implicit numerical scheme, i.e.,

$$[x_{k+1} - x_k]/\Delta t = F_{\psi,E}(x_{k+1},u_k), \quad (10)$$

where x_k and u_k denote the state and control input, respectively, at the time step t_k, x_{k+1} denotes the state at the next time step t_{k+1} and Δt is the simulation time step. The magnetic and thermal state evolution can be obtained by iteratively solving (10) at each time step from a given initial condition at time t_0, i.e., $x_0 = x(t_0)$.

3.3 Control Actuator Trajectory Parameterization

We parameterize the trajectories of the i-th control actuator (u_i) by a finite number of parameters (n_{p_i}) at discrete points in time (t_{p_i}), i.e., $t_{p_i} = [t_0,t_1,\ldots,t_k,\ldots,t_k = t_f] \in \mathbb{R}^{n_{p_i}}$. During the time interval $t \in (t_k,t_{k+1})$ the i-th control input is determined by linear interpolation as $u_i(t) = u_i(t_k) + [u_i(t_{k+1}) - u_i(t_k)]\,(t-t_k)/(t_{k+1}-t_k)$. By combining all of the parameters utilized to represent each individual actuator trajectory into a vector

$$\tilde{\theta} = \left[u_1^1,\ldots,u_1^{n_{p_1}},\ldots,u_i^1,\ldots,u_i^{n_{p_i}},\ldots,u_{n_{act}}^1,\ldots,u_{n_{act}}^{n_{p_{n_{act}}}}\right], \quad (11)$$

where $\tilde{\theta} \in \mathbb{R}^{n_p^{tot}}$ and $n_p^{tot} = \sum_{i=1}^{n_{act}} n_{p_i}$, we can write the parameterized control actuator trajectories as

$$u(t) = \Pi(t)\tilde{\theta}, \quad (12)$$

where $\Pi(t) \in \mathbb{R}^{n_{act}\times n_p^{tot}}$ is a piecewise linear function of time. Some of the parameters in the vector (11) may be chosen to be fixed due to the desire to obtain an operating condition at the time t_f with a specific set of characteristics (a final plasma current ($I_p(t_f)$) and/or line-averaged electron density ($\bar{n}_e(t_f)$)), or to provide the ability to acquire diagnostic data (constant power in a neutral beam launcher). Therefore, the subset of free parameters in the vector (11) can be combined into a vector of to-be-optimized parameters which we define as $\theta \in \mathbb{R}^{n_{opt}}$ where $n_{opt} \le n_p^{tot}$.

3.4 Actuator Constraints

The actuator magnitude and rate constraints are given by

$$I_p^{min} \le I_p(t) \le I_p^{max}, \quad (13)$$
$$P_{ec}^{min} \le P_{ec_i}(t) \le P_{ec}^{max}, \quad i = 1,\ldots,n_{ec} \quad (14)$$
$$P_{nbi}^{min} \le P_{nbi_i}(t) \le P_{nbi}^{max}, \quad i = 1,\ldots,n_{nbi} \quad (15)$$
$$-I_{p,max}^{d'} \le dI_p/dt \le I_{p,max}^{u'}, \quad (16)$$

where $(\cdot)^{min}$ and $(\cdot)^{max}$ are the minimum and maximum limits, respectively, and $I_{p,max}^{d'}$ and $I_{p,max}^{u'}$ are the maximum total plasma current ramp-down and ramp-up rates, respectively. The actuator constraints (13)-(16) can be combined together and written in terms of the to-be-optimized parameters θ in a compact matrix form as

$$A_u^{lim}\theta \le b_u^{lim}. \quad (17)$$

3.5 Plasma State and MHD Stability Contraints

The MHD stability limit related to the plasma magnetic states considered in this work is expressed as

$$q_{min}(t) \ge q_{min}^{lim}, \quad (18)$$

where $q_{min}(t) = \min\{q(\hat{\rho},t)\}$ and q_{min}^{lim} is a constant chosen to be slightly greater than one to avoid the onset of sawtooth oscillations (Wesson (2004)). In order for the plasma to remain in the H-mode operating regime, the net power across the plasma surface, P_{net}, must be greater than a threshold power (Martin et al. (2008)), $P_{threshold}$, i.e.,

$$P_{net}(t) \ge P_{threshold}(t), \quad (19)$$

where $P_{net}(t) = P_{tot}(t) - dE/dt = E/\tau_E(t)$. The final MHD stability limit considered in this work is given by

$$\bar{n}_{e20}(t) \leq n_g(t), \tag{20}$$

where $\bar{n}_{e20}(t)$ is the line-averaged electron density evaluated in units of 10^{20} m^{-3} and $n_g(t) = I_p(t)[\text{MA}]/\pi a^2$ is referred to as the Greenwald density limit (Greenwald et al. (1988)). We next chose to formulate the constraints (18)-(19) as integral constraints (Teo et al. (1991)). This provides us the ability to reduce the number of constraints imposed on the optimization problem solution. An example of this is given for the constraint (18) as

$$c_q^{lim} = \int_{t_0}^{t_f} \max\{0, q_{min}^{lim} - q_{min}(t)\}dt \leq 0. \tag{21}$$

The MHD stability constraint (19) can be written in the form of (21) and combined together and written in a compact matrix form as

$$c_{mhd}^{lim}(x(t)) \leq 0. \tag{22}$$

As the MHD stability constraint (20) depends directly on the to-be-optimized parameters θ, it is included in the formulation of the actuator constraints (17).

3.6 Optimization Problem Statement and Solution Method

The nonlinear, constrained, actuator trajectory optimization problem is now to determine the to-be-optimized parameters θ that minimize the cost functional (8) subject to the plasma dynamics (9), the control actuator trajectory parameterization (12), the actuator constraints (17), and the plasma state and MHD stability constraints (22). This optimization problem is written mathematically as

$$\min_{\theta} \quad J(t_f) = J(\dot{x}(t_f), x(t_f)), \tag{23}$$

such that

$$\begin{aligned} \dot{x} &= F_{\psi,E}(x,u) & A_u^{lim}\theta &\leq b_u^{lim}, \\ u(t) &= \Pi(t)\tilde{\theta} & c_{mhd}^{lim}(x(t)) &\leq 0. \end{aligned} \tag{24}$$

We solve this optimization problem by employing a method called sequential quadratic programming (SQP) (Nocedal and Wright (2006)). The SQP solution method is predicated on determining a local minimizer of the nonlinear program (NLP) (23)-(24) by iteratively solving a sequence of quadratic programs (QP). At each iteration we have a current estimate of a local minimizer of the NLP and a QP which minimizes a quadratic approximation of the original system Hamiltonian subject to a linear approximation of the system constraints around the current estimate. The solution of each QP then yields a step toward the solution of the original NLP.

We provide an overview of the SQP solution method for a general NLP defined by

$$\min_{v} \quad \mathcal{J}(z,v) \quad \text{such that} \quad f(z,v) = 0. \tag{25}$$

To simplify the explanation of the SQP technique, we only consider equality constraints of the form shown in (25). We begin by defining the system Hamiltonian as $\mathcal{H}(z,v,\lambda) = \mathcal{J}(z,v) + \lambda^T f(z,v)$, where λ is a to-be-determined Lagrange multiplier. An incremental change in the Hamiltonian with respect to changes in the parameters is given to first order by $d\mathcal{H} = \mathcal{H}_z dz + \mathcal{H}_v dv + \mathcal{H}_\lambda d\lambda$, where $(\cdot)_i = \frac{\partial(\cdot)}{\partial i}$ for $i \in \{z, v, \lambda\}$. At a local minimum (z^*, v^*, λ^*), $d\mathcal{H}$ must be zero for all increments dz, dv, $d\lambda$. Therefore, the first-order optimality conditions for the NLP (25) are given by the nonlinear equations

$$\begin{aligned} \mathcal{H}_z(z^*,v^*,\lambda^*) &= \mathcal{J}_z(z^*,v^*) + (\lambda^*)^T f_z(z^*,v^*) = 0, \\ \mathcal{H}_v(z^*,v^*,\lambda^*) &= \mathcal{J}_v(z^*,v^*) + (\lambda^*)^T f_v(z^*,v^*) = 0, \\ \mathcal{H}_\lambda(z^*,v^*,\lambda^*) &= f(z^*,v^*) = 0. \end{aligned} \tag{26}$$

One approach to solving the NLP (25) is to assume we have an iteration $\left(z^{(k+1)}, v^{(k+1)}, \lambda^{(k+1)}\right) = \left(z^{(k)}, v^{(k)}, \lambda^{(k)}\right) + \left(\zeta^{(k)}, \xi^{(k)}, \sigma^{(k)}\right)$ that is converging to the solution (z^*, v^*, λ^*) of (26), where $(\zeta^{(k)}, \xi^{(k)}, \sigma^{(k)})$ are search directions. If the current estimate $(z^{(k)}, v^{(k)}, \lambda^{(k)})$ is close to (z^*, v^*, λ^*), we can linearize (26) around $(z^{(k)}, v^{(k)}, \lambda^{(k)})$, i.e.,

$$\begin{aligned} 0 =& \mathcal{H}_z(z^{(k)},v^{(k)},\lambda^{(k)}) + \mathcal{H}_{zz}(z^{(k)},v^{(k)},\lambda^{(k)})\zeta^{(k)} \\ &+\mathcal{H}_{zv}(z^{(k)},v^{(k)},\lambda^{(k)})\xi^{(k)} + \mathcal{H}_{z\lambda}(z^{(k)},v^{(k)},\lambda^{(k)})\sigma^{(k)}, \\ 0 =& \mathcal{H}_v(z^{(k)},v^{(k)},\lambda^{(k)}) + \mathcal{H}_{vz}(z^{(k)},v^{(k)},\lambda^{(k)})\zeta^{(k)} \\ &+\mathcal{H}_{vv}(z^{(k)},v^{(k)},\lambda^{(k)})\xi^{(k)} + \mathcal{H}_{v\lambda}(z^{(k)},v^{(k)},\lambda^{(k)})\sigma^{(k)}, \\ 0 =& \mathcal{H}_\lambda(z^{(k)},v^{(k)},\lambda^{(k)}) + \mathcal{H}_{\lambda z}(z^{(k)},v^{(k)},\lambda^{(k)})\zeta^{(k)} \\ &+\mathcal{H}_{\lambda v}(z^{(k)},v^{(k)},\lambda^{(k)})\xi^{(k)} + \mathcal{H}_{\lambda\lambda}(z^{(k)},v^{(k)},\lambda^{(k)})\sigma^{(k)}, \end{aligned} \tag{27}$$

where $(\cdot)_{ij} = \frac{\partial^2(\cdot)}{\partial i \partial j}$ for $i \in \{z, v, \lambda\}$ and $j \in \{z, v, \lambda\}$. From (26), we note that $\mathcal{H}_{z\lambda} = \mathcal{H}_{\lambda z} = f_z$, $\mathcal{H}_{v\lambda} = \mathcal{H}_{\lambda v} = f_v$, and $\mathcal{H}_{\lambda\lambda} = 0$, which allows us to write (27) as

$$\left.\begin{bmatrix} \mathcal{H}_{zz} & \mathcal{H}_{zv} & f_z \\ \mathcal{H}_{vz} & \mathcal{H}_{vv} & f_v \\ f_z & f_v & 0 \end{bmatrix}\right|_{(z^{(k)},v^{(k)},\lambda^{(k)})} \begin{bmatrix} \zeta^{(k)} \\ \xi^{(k)} \\ \sigma^{(k)} \end{bmatrix} = - \left.\begin{bmatrix} H_z \\ H_v \\ f \end{bmatrix}\right|_{(z^{(k)},v^{(k)},\lambda^{(k)})} \tag{28}$$

The search directions $(\zeta^{(k)}, \xi^{(k)}, \sigma^{(k)})$ can then be obtained by solving (28). It can be shown that the first-order optimality condition of the QP

$$\min_{\xi^{(k)}} \quad \mathcal{L}(\zeta^{(k)}, \xi^{(k)})\big|_{(z^{(k)},v^{(k)},\lambda^{(k)})}, \tag{29}$$

such that

$$f(z^{(k)}, v^{(k)}) + [f_z \quad f_v]\big|_{(z^{(k)},v^{(k)})} \begin{bmatrix} \zeta^{(k)} \\ \xi^{(k)} \end{bmatrix} = 0, \tag{30}$$

where

$$\mathcal{L} = \mathcal{H} + [\mathcal{H}_z \quad \mathcal{H}_v] \begin{bmatrix} \zeta^{(k)} \\ \xi^{(k)} \end{bmatrix} + \frac{1}{2} \begin{bmatrix} \zeta^{(k)} & \xi^{(k)} \end{bmatrix} \begin{bmatrix} \mathcal{H}_{zz} & \mathcal{H}_{zv} \\ \mathcal{H}_{vz} & \mathcal{H}_{vv} \end{bmatrix} \begin{bmatrix} \zeta^{(k)} \\ \xi^{(k)} \end{bmatrix},$$

with Lagrange multiplier $\sigma^{(k)}$, is given by (28). Search directions for the NLP (25) can then be obtained from the sequence of quadratic programs (29)-(30), which represent a quadratic approximation of $\mathcal{H}$ subject to a linear approximation of f around the current estimate $(z^{(k)}, v^{(k)}, \lambda^{(k)})$.

4. OPTIMIZED ACTUATOR TRAJECTORIES

We now solve the actuator trajectory optimization problem (23)-(24) to reach a target plasma state (such that the achieved state is in a stationary condition) at a time t_f during the plasma discharge by employing the SQP solution method. The optimization is carried out over the time interval $t_{opt} = t \in [t_0, t_f] = [0.5, 3.0]$ sec. The auxiliary H&CD actuators on DIII-D considered in this work are 6 gyrotron launchers and 6 co-current neutral beam injectors (NBI), which are referred to by the names [30L/R,150L/R,330L/R], where L and R denote left and right NBI lines, respectively. In the H&CD scheme considered, the gyrotrons inject power into the plasma in the spatial region $\hat{\rho} \in [0.3, 0.7]$, the 30L/R and 330L/R NBI lines inject power into the plasma with a deposition profile

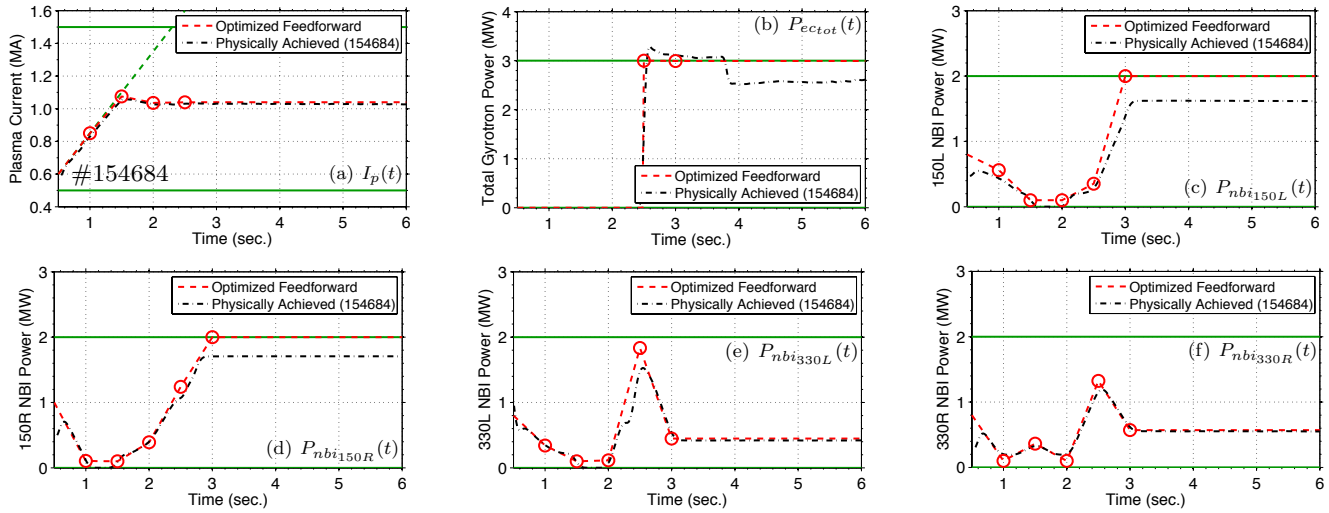

Fig. 1. Optimized and physically achieved (DIII-D shot 154684) actuator trajectories: (a) total plasma current, (b) total gyrotron launcher power, and (c-f) individual neutral beam injection powers. Note: optimized parameter (red ∘) and magnitude (solid green) and rate (dash green) limits applied on numerical solution of optimization problem.

that is peaked in the center of the plasma (referred to as on-axis NBI), and the 150L/R NBI lines inject power into the plasma with a deposition profile that is peaked in the spatial region $\hat{\rho} \in [0.3, 0.5]$ (referred to as off-axis NBI) (Barton et al. (2013)).

We begin by parameterizing the i-th actuator trajectory by $n_{p_i} = 6$ discrete parameters at the time points $t_{p_i} = [0.5, 1.0, \ldots, 3.0]$ sec. and choosing the fixed parts of the parameter vector (11). Firstly, the total gyrotron power, $P_{ec_{tot}}(t)$, is chosen to be evenly distributed amongst the individual gyrotron launchers. Additionally, as the gyrotrons have a limited amount of total energy they can deliver in a plasma discharge, they are set to be inactive during the time interval $t \in [0.5, 2.5)$ sec. so they have the potential to be used at full power for the remainder of the discharge. Secondly, in order to acquire diagnostic data to reconstruct the q-profile, the 30L/R neutral beam powers are fixed at 1.1 MW. Thirdly, the line-averaged electron density trajectory is chosen to be fixed (linearly ramped-up from an initial value $\bar{n}_e(0.5) = 2 \times 10^{19}$ m^{-3} to a final value $\bar{n}_e(2.0) = 4.2 \times 10^{19}$ m^{-3} and then held constant) because density control is challenging in experiments due to large particle recycling at the tokamak wall. Finally, all of the actuator values at the initial time t_0 and the value of the total plasma current at the time t_f are chosen to be fixed. The vector of to-be-optimized parameters is then given by

$$\theta = \big[P_{ec_{tot}}(2.5), P_{ec_{tot}}(3.0), P_{nbi_i}(1.0), \ldots, P_{nbi_i}(3.0), I_p(1.0), \ldots, I_p(2.5)\big], \quad (31)$$

where $i \in$ [150L/R,330L/R], respectively.

The optimized parameters (31) (and associated actuator trajectories) determined by solving the optimization problem (23)-(24), with the target plasma state ($q^{tar}(\hat{\rho})$ and β_N^{tar}) chosen to be the q-profile and β_N experimentally achieved at 3.0 sec. in DIII-D shot 150320, are shown in Fig. 1. Firstly, the total plasma current (I_p) trajectory is ramped up at the maximum allowable rate and exhibits a slight overshoot before settling to the specified final value. Secondly, the off-axis NBI power ($P_{nbi_{150L/R}}$) is gradually increased up to the maximum allowable value during the time interval $t \in [1.5, 3]$ sec. to set up a stationary state with off-axis auxiliary current-drive, which is needed to achieve the target q-profile in the plasma core. Thirdly, the maximum amount of gyrotron power ($P_{ec_{tot}}$) is applied with the same objective as well as to reach the target β_N. Finally, a moderate amount of on-axis NBI power ($P_{nbi_{330L/R}}$) is applied during the time interval $t \in [2, 3]$ sec. to set up a stationary state before settling to a relatively small amount that is needed to achieve the target β_N.

5. SIMULATION AND EXPERIMENTAL TESTING OF OPTIMIZED ACTUATOR TRAJECTORIES

The optimized actuator trajectories shown in Fig. 1 are now tested through simulation with the physics-based model discussed in Section 2 and experimentally in the DIII-D tokamak during shot 154684. As the optimized trajectories are designed to achieve a target plasma state at the time $t_f = 3.0$ sec. in such a way that the achieved state is as stationary in time as possible, the actuator values are held constant from the time t_f until the end of the plasma discharge. It is important to note that the optimized trajectories represent the references to dedicated control loops that command the physical actuators on DIII-D. As shown in Fig. 1, the dedicated control loops were able to follow the requested trajectories reasonably well. However, during DIII-D shot 154684, one of the gyrotrons faulted at approximately 3.8 sec., the 150R neutral beam injector was saturated at its upper limit after 2.75 sec., and the dedicated control loop commanding the 150L neutral beam injector was not able to follow the request after 2.5 sec.

Time traces of q in the plasma core and of β_N and a comparison of the target, physics-based model predicted, and experimentally achieved q-profiles at various times is shown in Fig. 2. As shown, the optimized trajectories were able to drive the experimental plasma as close as possible to the desired stationary q-profile at 3.0 sec. despite the limitations of the dedicated control loops on following the requested trajectories. However, at approximately 2.3 sec., MHD instabilities developed and persisted for the remainder of the discharge. The MHD modes degraded the plasma confinement characteristics (shown in the immediate reduction of β_N once the modes develop) and result

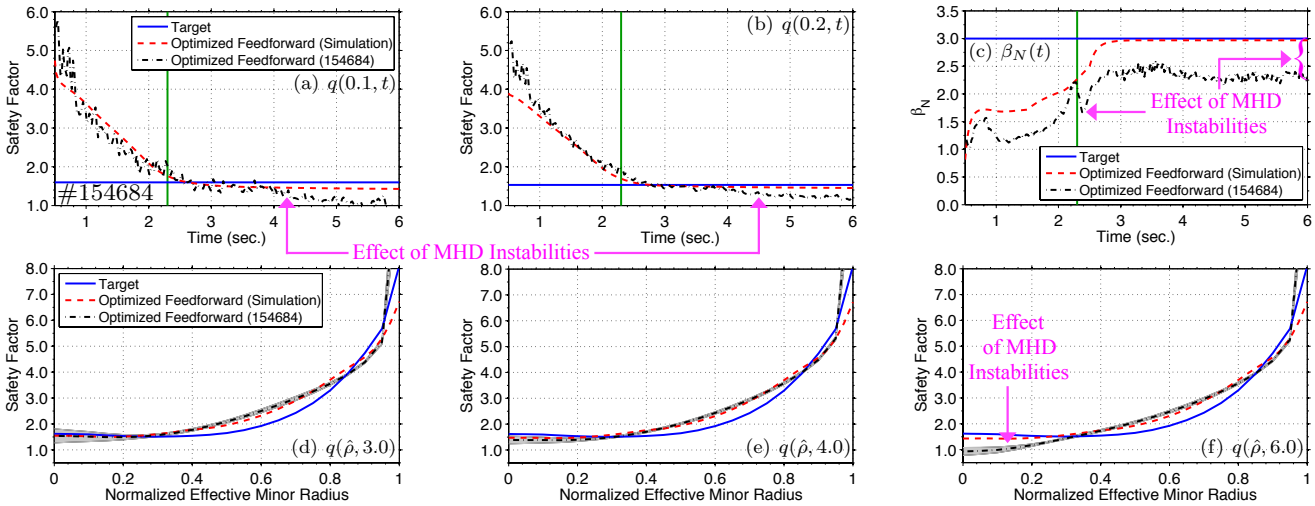

Fig. 2. Simulation and experimental (DIII-D shot 154684) testing of optimized actuator trajectories: (a-c) time trace of q in the plasma core and of β_N and (d-f) q-profile at various times. The solid green line denotes the onset of MHD instabilities during DIII-D shot 154684. Approximate error bars for the measured q-profiles (obtained from the real-time EFIT equilibrium reconstruction code (Ferron et al. (1998))) are shown by the gray-shaded regions.

in the inability to experimentally achieve the target β_N and maintain the target q-profile in the plasma core after approximately 4.0 sec. However, through simulation with the physics-based model, it was shown that the optimized trajectories were able to steer the simulated plasma to the stationary target in the absence of MHD modes.

6. CONCLUSIONS AND FUTURE WORK

A numerical optimization algorithm was developed to complement the experimental effort of advanced scenario planning in the DIII-D tokamak. At the core of the optimization algorithm is a nonlinear, physics-based, control-oriented model of the plasma dynamics. One direction of future work is to extend the physics-based model by coupling the poloidal magnetic flux profile dynamics together with the distributed dynamics of the plasma electron temperature profile in order to better represent the effect the q-profile has on plasma transport. The optimized actuator trajectories were successfully tested through simulation, and a preliminary experimental test in DIII-D demonstrated the ability of the optimized trajectories to steer the plasma to a target stationary q-profile. However, as observed in the experiment, access to advanced operating scenarios can be limited by the triggering of MHD instabilities. Therefore, a second direction of future work is to formulate additional plasma state constraints that can be imposed on the solution of the optimization problem to maintain distance from critical MHD stability limits. A third direction of future work is additional experimental testing of actuator trajectories determined by solving the optimization algorithm to further validate the presented approach. Additionally, the optimization algorithm will be utilized to study the achievability of target plasma states with different H&CD schemes. Finally, as a result of the MHD instabilities that developed during the experimental test, the optimized feedforward trajectories were not able to achieve the target β_N and maintain a stationary q-profile for the entirety of the plasma discharge. Therefore to account for external plasma disturbances (such as the observed reduction in confinement) and actuation limitations (either in actuator regulation or actuator faults), the optimized feedforward trajectories should be further integrated together with a feedback control scheme to improve the ability to robustly achieve plasma target conditions.

REFERENCES

J. E. Barton, W. Shi, K. Besseghir, J. Lister, A. Kritz, E. Schuster, et al. Physics-based control-oriented modeling of the safety factor profile dynamics in high performance tokamak plasmas. In *52nd IEEE Conference on Decision and Control*, pages 4182–4187, 2013.

F. Felici et al. Nonlinear model-based optimization of actuator trajectories for tokamak plasma profile control. *Plasma Phys. and Control. Fusion*, 54:025002, 2012.

J. Ferron et al. Real time equilibrium reconstruction for tokamak discharge control. *Nucl. Fusion*, 38:1055, 1998.

M. Greenwald et al. A new look at density limits in tokamaks. *Nuclear Fusion*, 28:2199, 1988.

F. Hinton and R. Hazeltine. Theory of plasma transport in toroidal confinement systems. *Rev. Mod. Phys.*, 48: 239–308, 1976.

ITER Physics Basis. *Nuclear Fusion*, 39:2137, 1999.

Y. Martin et al. Power requirements for accessing the H-mode in ITER. *Journal of Physics: Conference Series*, 123:012033, 2008.

J. Nocedal and S. J. Wright. *Numerical optimization*. Springer, New York, 2006.

Y. Ou, C. Xu, E. Schuster, et al. Design and simulation of extremum-seeking open-loop optimal control of current profile in the DIII-D tokamak. *Plasma Phys. and Control. Fusion*, 50:115001, 2008.

A. G. Peeters. The bootstrap current and its consequences. *Plasma Phys. and Control. Fusion*, 42:B231–B242, 2000.

T. Taylor et al. Physics of advanced tokamaks. *Plasma Phys. and Control. Fusion*, 39:B47–B73, 1997.

K. Teo et al. *A unified computational approach to optimal control problems*. Wiley, New York, 1991.

J. Wesson. *Tokamaks*. Oxford, UK: Clarendon Press, 2004.

C. Xu, Y. Ou, J. Dalessio, E. Schuster, et al. Ramp-up phase current profile control of tokamak plasmas via nonlinear programming. *IEEE Transactions on Plasma Science*, 38:163–173, 2010.